PHYSICAL REVIEW B VOLUME 58, NUMBER 7 15 AUGUST 1998-I

Oxidation of Sn overlayers and the structure and stability of Sn oxide films on Pd(111)

Adam F. Lee* and Richard M. Lambert†
Department of Chemistry, University of Cambridge, Lensfield Road, Cambridge CB2 1EW, United Kingdom
(Received 22 July 1997; revised manuscript received 6 May 1998)

The oxidation at 300 K of ultrathin Sn films has been studied by Auger and x-ray photoelectron spectroscopy. The process divides into two regimes: submonolayer Sn coverages are stable towards low ($<10^5$ L) oxygen exposures, becoming fully oxidized to stoichiometric SnO at higher exposures ($\sim 10^{11}$ L). Thicker Sn deposits oxidize more rapidly, and analysis of the Sn Auger parameter and substrate surface core-level shift indicates that oxidation is accompanied by relatively little change in the initial state charge density of the Sn atoms. This reflects strong preexisting Sn to Pd charge transfer and the low dimensionality of the oxidized Sn overlayers. Thermal stability of these films increases with thickness and they decompose by evolution of gaseous oxygen accompanied by Pd/Sn surface alloy formation. The strong Pd-Sn chemical bond exerts a controlling influence on both overlayer oxidation and oxide decomposition processes within the Sn/Pd(111) system. [S0163-1829(98)11631-4]

I. INTRODUCTION

Much of the current interest in tin oxides and Pd/tin oxide systems stems from their important technological role in, e.g., high conductivity heat reflectors, gas sensors,[1,2] and catalysts.[3,4] Palladium is an important promoter in tin oxide gas-sensing devices, and is in itself a major industrial catalyst for hydrogenation and combustion chemistry. The present study is motivated by our recent research on novel Pd/Sn bimetallic catalysts prepared by encapsulating Pd clusters with Sn.[5] The resulting bimetal catalysts have a core-shell structure and are sensitive to oxidation of the Sn "skin." Reduction of the Sn oxide layer yields highly efficient catalysts. In order to gain insight into the mechanisms of Sn oxide formation and decomposition, and the possible role of Pd/Sn surface alloying in these structures, we have studied the corresponding properties of Sn overlayers grown on a Pd(111) substrate.

The oxidation of Sn particles, thin films, and bulk samples has been the subject of numerous investigations over the past 30 years, despite which contradictory findings are still reported for many aspects of the oxidation process. To a large extent, this controversy arises from difficulties in identifying and distinguishing the different tin oxides, although several recent studies on "bulk" oxide samples have reached a consensus regarding the identification and discrimination of Sn(II) and Sn(IV) oxidation states.[6,7] Furthermore, tin oxidation has been studied over a wide range of substrates and conditions, prohibiting ready comparison.

An early electron microscopy study by Boggs *et al.*[8] suggested that oxygen chemisorption on Sn resulted in SnO formation. The first detailed UPS study by Powell and Spicer[9] of evaporated thick Sn films on Mo/stainless-steel substrates showed valence-band (VB) features attributed to SnO_2 following a "saturation" exposure of 4000 L. Additional work-function measurements suggested oxygen penetration beneath the surface, leaving a metallic Sn overlayer (also proposed by Stander[10]). Interestingly, subsequent electron energy loss spectroscopy (EELS) measurements by Powell[11] on polycrystalline Sn exposed to 5000 L O_2 indicated the presence of Sn and SnO, but *not* SnO_2. This discrepancy was attributed to the shorter sampling depth of EELS versus ultraviolet photoelectron spectroscopy (UPS), and the presence of SnO_2 beneath a thin SnO layer (more recently propounded by Asbury and Hoflund[12]). Lau and Wertheim[13] published VB spectra from a Sn foil exposed to 10^6 L O_2 possessing both SnO and SnO_2-like features, suggesting a mixed oxide surface.

Efforts to discriminate the two oxides using alternative photoemission measurements have also proved contentious, with Powell,[11] Lin,[14] and Wagner[15] reporting identical Sn Auger electron spectroscopy (AES) shifts for SnO and SnO_2, while Sen *et al.*[16] observed a 4 eV difference. This may reflect the widely differing substrates (powders, evaporated films, and polycrystalline foils) and preparative techniques employed in these studies. The latter authors[16] proposed that oxidation initially proceeds through SnO formation, with an SnO_2 overlayer emerging at saturation exposures—the inverse of Powell's hypothesis. A similar model was proposed in an AES/low-energy electron loss spectroscopy (LEELS) study by Bevolo *et al.* for the oxidation by gaseous oxygen of electrochemically etched polycrystalline and single-crystal Sn surfaces,[17] wherein SnO_2 surface enrichment is observed (albeit following only a 50 L O_2 exposure), with both oxides coexisting subsurface at higher exposures of $\sim 10^7$ L. The various models for Sn oxidation came full circle with Woods and Hopkins' AES and EELS study on a stepped β-Sn(001) surface,[18] which reported the formation of a thin SnO overlayer following saturation oxygen exposures (<4000 L), as suggested 24 years earlier by Boggs *et al.*[8]

Two more recent papers on Sn oxidation at very high oxygen exposures using EELS (Ref. 7) and UPS,[19] respectively, suggest that the initial low-pressure stage of oxidation proceeds via surface SnO formation. However, in the angle-resolved EELS study of Hoflund *et al.*[7] a subsurface transitional oxide, intermediate between SnO and SnO_2, is proposed after 500 L O_2, which synchrotron valence-band measurements by De Padova *et al.*[19] failed to detect. (Intermediate tin oxide stoichiometries have also been reported during high-temperature calcination of dispersed Sn/Al_2O_3 catalysts[20] and studies on polycrystalline tin oxide films by Cox *et al.*[6]) Both Refs. 7 and 19 confirm the presence of SnO

0163-1829/98/58(7)/4156(10)/$15.00 PRB 58 © 1998 The American Physical Society

and SnO_2 following high oxygen pressures, but differ regarding their relative depth distribution, reflecting differences in the surface sensitivity of UPS versus EELS.

Here it is found that high-pressure, room-temperature oxidation of Sn thin films results exclusively in SnO formation, in the absence of intermediate or higher oxides. Diffusion-limited oxygen transport, facilitated by a strong substrate-Sn interaction, stabilizes a metallic Sn phase at the Pd-Sn interface, promoting subsequent thermally induced Pd/Sn surface alloying.

II. EXPERIMENTAL METHODS

Experiments were performed in a combined XPS/environmental cell apparatus described previously[21] operated at a base pressure of 1×10^{-10} Torr. The Pd(111) sample could be resistively heated to 1200 K, and cleaning was achieved by cycles of Ar^+ sputtering (6×10^{-2} A m^{-2}, 500 eV) and annealing at 800 K. XPS and x-ray excited Auger spectra (XAES) were acquired using Mg $K\alpha$ radiation (1253.6 eV) in conjunction with a VSW HA100 single channel analyzer. Electron- and x-ray excited Auger spectra were recorded in $N(E)$ mode and electronically differentiated for quantitative analysis. The analyzer take-off angle was 45° and both excitation sources were incident at 45° to the surface normal. Sn deposition was performed at 300 K by means of a collimated, resistively heated alumina crucible.[22] Subsequent oxidation was also carried out at 300 K. Quoted Sn coverages were derived by reference to the Sn monolayer coverage ($\sim9\times10^{14}$ atom cm^{-2}) obtained from photoemission uptake curves. Total surface contamination due to the principal impurities (C, S, and Cl) was <0.1 ML, even for the thickness Sn films and highest oxygen exposures.

Oxygen (Distillers 4.6) exposures up to 10^4 L ($1\ L=1\times10^{-6}$ Torr s) were achieved in flowing gas at pressures between 1×10^{-7} and 1×10^{-5} Torr. 10^5 L exposure was achieved in a static system with an O_2 pressure of 10^{-4} Torr. Higher O_2 doses necessitated *in situ* sample transfer to a preconditioned environmental cell, where static O_2 pressures of 250 Torr provided exposures up to 5×10^{10} L over a reasonable time scale. The Pd and Sn *MVV* and O *KLL* AES transitions at 330, 430, and 510 eV kinetic energy (KE) were monitored, together with the corresponding $3d$ and $1s$ photoemission peaks at 335, 484, and 522 eV binding energy (BE), respectively. All XP spectra were recorded at 22 eV pass energy, with the exception of valence-band measurements, which were taken at 44 eV pass energy. Peak analysis of XP spectra was performed following subtraction of a Shirley background using least-squares fitting procedures.

Oxygen surface atom coverages were determined quantitatively by reference to the O *KLL* Auger and $1s$ XP intensities measured for the saturation $p(2\times2)$O-Pd(111) structure. While this calibration will introduce inaccuracies for thick tin oxide films due to inelastic scattering processes, such errors are negligible for the very thin oxide films considered in this study in view of the inelastic mean-free path of oxygen photoelectrons concerned (~9 Å). Additional agreement with quoted O_a exposures was obtained by calibration against the high-pressure (1×1)O-Pd(111) phase.

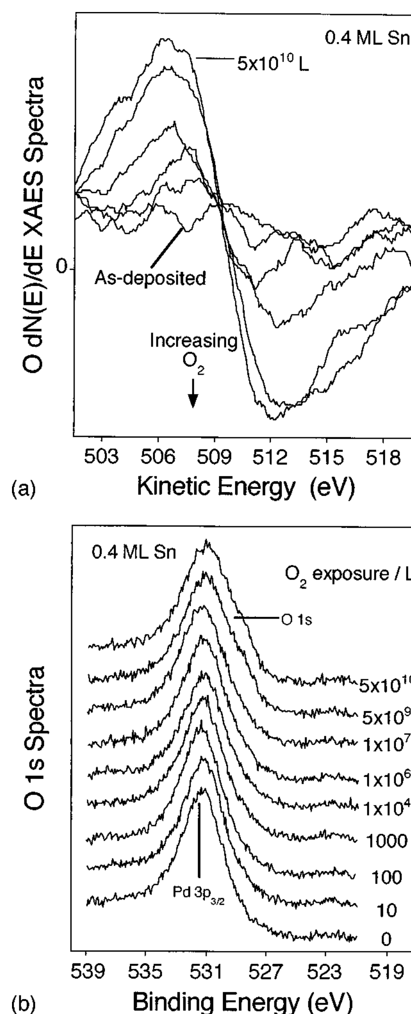

FIG. 1. (a) O $dN(E)/dE$ *KLL* Auger and (b) O $1s$ XP spectra as a function of oxygen exposure for a 0.4 ML Sn film.

III. OXIDATION OF SN SN OVERLAYERS

Room-temperature exposure of Pd-supported Sn films to between 1 and 5×10^{10} L O_2 induced significant oxidation, as shown by the growth in O XAES and XPS intensities [Figs. 1(a) and 1(b), respectively]. The O $1s$ transition appears as a low BE shoulder at ~529 eV on the Pd $3p_{3/2}$ peak (531 eV) and remains unresolved even for the highest oxygen doses. This value is somewhat lower than the O $1s$ binding energies reported for extended SnO and SnO_2 films and high-purity polycrystalline powders, which range from 529.7 eV (Ref. 23) to 531.4 eV,[24] and may reflect the low dimensionality of our oxide sample.

The rate of oxidation was dependent on both oxygen exposure and Sn overlayer thickness. Oxygen uptake was undetectable at exposures below 10 L; higher exposures resulted in the emergence of oxygen photoemission features for both submonolayer and multilayer Sn deposits. Over submonolayer films, for exposures between 10 and 10^5 L, oxygen uptake proceeded in a slow, logarithmic fashion followed by rapid oxidation, which continued up to the maximum dose of 5×10^{10} L. In contrast, with multilayer Sn films, the oxygen XP intensities rose rapidly at low exposures, attaining ~90% of their limiting values after only 10^5 L O_2 (Fig. 2). For a 0.4 ML Sn deposit, a similar oxygen

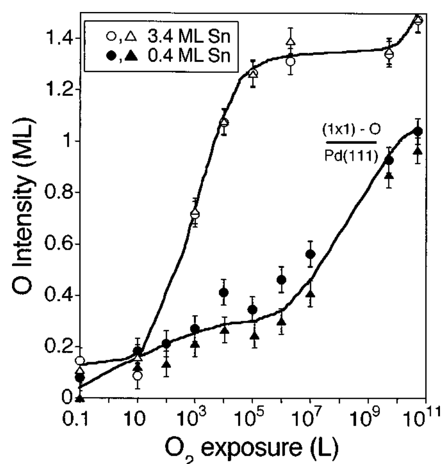

FIG. 2. Combined O XAES (○,●)/1s(△,▲) intensities vs oxygen exposure for 0.4 and 3.4 ML Sn films.

exposure resulted in the O 1s intensity reaching only one-third of the corresponding limiting value. On clean Pd(111) saturation oxygen uptake under UHV conditions corresponds to a (2×2) structure, i.e., 0.25 ML, in agreement with the literature.[25] Control experiments with the clean surface at elevated pressures ($>10^{-4}$ Torr) showed that the overlayer adatom density can be increased to ~1 ML.

The oxygen incorporated within these Sn/Pd surfaces is associated with surface tin oxide formation, and is not due to oxidation of the Pd selvedge. First, the corresponding Sn AES and XP data show pronounced changes in both peak shape and energy as a function of oxygen exposure between 1 and 5×10^{10} L (Figs. 3 and 4). The large decrease in the Sn *MNN* kinetic energy (>2 eV) and associated peak broadening following exposures $>1\times10^{5}$ L O_2 is consistent with observations on the oxidation of polycrystalline Sn foils at $>10^{-6}$ Torr.[11,16,26] Ultrathin (<10 ML) Sn films grown on Au(111) behave in a similar fashion.[27] Equally, the increase in Sn $3d_{3/2,5/2}$ core level BE (from 484.6 eV) with oxygen exposure (in particular that for multilayer films) and the limiting shift of ~1 eV are consistent with those reported for oxidation of Sn foils,[19,28] which results in stoichiometric,

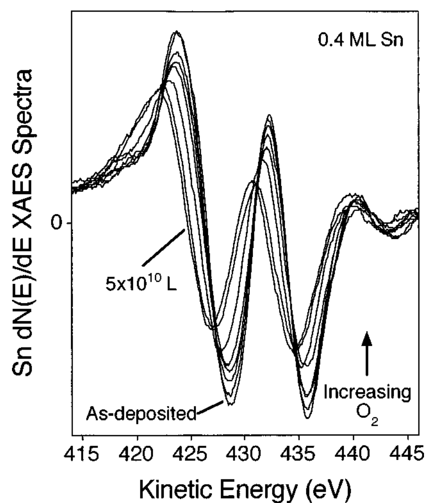

FIG. 3. Sn $dN(E)/dE$ *MNN* Auger spectra vs oxygen exposure for 0.4 ML Sn film.

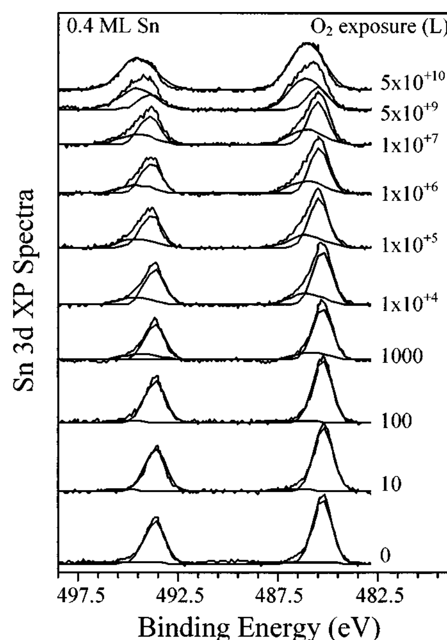

FIG. 4. Sn 3d XP spectra vs oxygen exposure for 0.4 ML Sn film. Fitted metal and oxide Gaussian components are also shown.

possibly transitional, tin oxide surface structures, rather than chemisorbed oxygen overlayers. Indeed the most recent XP study of tin foil oxidation[19] reports Sn 3d BE shifts of between 1 and 2.5 eV during formation of surface tin oxides. (Note that while a spread of values is reported in the literature for the Sn 3d and O 1s BE of bulk oxides, the values found here are somewhat lower. We attribute this difference to the low dimensionality of our as-deposited and oxidized overlayers, and *not* to energy referencing errors.)

Second, oxygen exposures above 10–100 L lift the Sn-induced substrate surface core-level shift (SCLS),[22] progressively restoring Pd XP features to their characteristic clean surface line shape, irrespective of Sn precoverage. The clean Pd SCLS arises from the reduced coordination of surface relative to bulk atoms. For metals possessing more than half-filled valence shells, the constraint that layerwise charge neutrality is maintained at the surface leads to an enhanced local surface Pd atom charge density and corresponding low binding energy surface XP transition.[29] The counteracting final-state core-hole screening contribution may be neglected for Pd(111). Charge transfer between thin Sn overlayers (≤2 ML) into the Pd(111) surface enhances the preexisting Pd SCLS by 0.25 eV,[22] increasing the full width at half maximum (FWHM) of Pd core levels. Lifting of this effect during Sn oxidation is exemplified by the changes in Pd $3d_{5/2}$ (335 eV BE) FWHM, Fig. 5. New substrate features were *not* observed for any oxygen exposure, discounting possible surface Pd oxide formation, which should in any case be negligible for oxygen pressures $<10^{-4}$ Torr and temperatures below 523 K.[30]

Although submonolayer Sn films are slower to oxidize than their multilayer counterparts, ultimately they are more completely oxidized, as determined by deconvolution of the Sn core-level spectra presented in Fig. 4 into metallic Sn^0 and oxidic Sn^{x+} components, Fig. 6. Prior to deconvolution using a least-squares-fitting routine, all spectra in Fig. 4 were subject to a factor analysis to determine the minimum num-

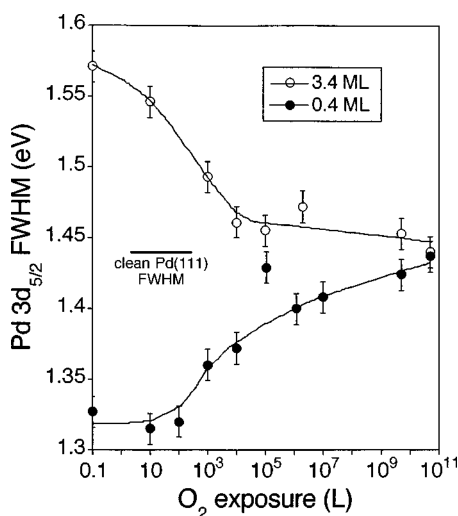

FIG. 5. Pd $3d$ FWHM vs oxygen exposure for 0.4 and 3.4 ML Sn films.

ber of independent components required to fit each Sn $3d$ spectrum. This analysis revealed that all spectra could be adequately fit by only one or two components. Subsequent peak deconvolution confirmed that good quality fits could be obtained using a single metallic Sn^0 and/or Sn^{x+} component. The properties of the metallic peak were determined from the as-deposited Sn film—a constant line shape and FWHM (1.1 eV) were used for all coverages, however it should be noted that the Sn metal position varies as a function of initial Sn coverage as documented.[22] Likewise, the properties of the oxide component (FWHM=2.0 eV) were determined from a 0.4 ML Sn film subject to the highest oxygen exposure, for which the metallic Sn contribution was negligible. Symmetric Gaussians were used for both Sn components (after De-Padova *et al.*[19]), and the spin-orbit ratio (5/2:3/2) was maintained at 1.5. The peak positions and thus separation of metal and oxide components were fixed (after Themlin *et al.*[31]). Similar factor analysis and deconvolution procedures applied to a 3.4 ML Sn film exposed to 5×10^{10} L O_2 indicate ~50% of surface Sn is retained in metallic form.

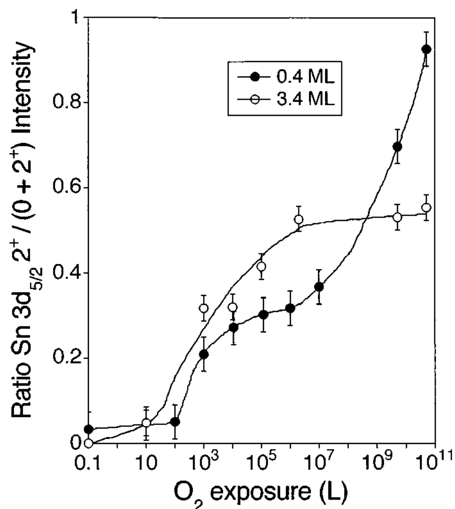

FIG. 6. Ratio of Sn^{2+}:Sn^0 $3d$ XP intensities vs oxygen exposure for 0.4 and 3.4 ML Sn films.

The very different oxidation kinetics of submonolayer and multilayer tin films may be rationalized as follows.

The resistance of submonolayer Sn deposits to low ($<1\times10^5$ L) O_2 exposures reflects Pd-Sn chemical bonding in the contact layer, also reported for Pt/Sn systems (Ref. 32 and references therein); it also points to the absence of significant atomic oxygen spillover from bare substrate patches. Evidence for such stabilization is provided by the eventual appearance of tin oxide photoemission features that coincide with lifting of the Sn-enhanced substrate SCLS (Ref. 22) (Fig. 5). The slow oxidation of submonolayer Sn deposits at exposures $<10^5$ L O_2 indicates these two-dimensional islands are themselves relatively inactive for low-pressure dissociative oxygen chemisorption. The small fraction of oxidic Sn present at these exposures may result from interaction of Sn island boundaries with O adatoms present on exposed Pd patches. However, this effect should reach a maximum ~10 L O_2 corresponding to the low-pressure ($<10^{-4}$ Torr) saturation of exposed Pd(111) sites [$\theta(O_a)=0.25$ ML]. The fact that it persists for exposures up to $\sim10^5$ L suggests that it is due to slow oxidation within the Sn islands.

Rapid oxidation of the remaining Sn atoms at higher oxygen pressures results in essentially total oxidation following a 5×10^{10} L O_2 exposure. Similar enhanced Sn oxidation rates are observed over polycrystalline Sn foil at exposures above 10^6 L O_2.[7,19] As in the present case, De Padova *et al.* observed continuous oxide growth following a plateau in the oxygen uptake between $\sim10^3$ and 10^6 L O_2. This change in oxidation kinetics was attributed to a transition from SnO to SnO_2 formation in the outermost oxide layers, facilitated by the presence of excess oxygen. Hoflund *et al.*[7] reached a similar conclusion; high-pressure oxidation results in the progressive accumulation and subsequent penetration of oxygen into the near-surface region, inducing the transformation of subsurface oxide to SnO_2. However, these studies report significant differences in the surface and/or subsurface distribution of stoichiometric Sn(II) and Sn(IV) oxides. Although in accord with both these studies we associate our oxidic Sn component with stoichiometric tin oxide formation, we find no evidence for such structural transformations during growth of the thin oxide films examined in this study. This is clear from the linear increase in surface concentration of the fitted oxidic Sn component with oxygen uptake, Fig. 7, which shows that a common oxide stoichiometry is maintained throughout the oxidation process. Since oxygen dissociation on Sn sites is most likely rate-determining in the oxidation of submonolayer Sn films where surface→bulk diffusion processes are absent, and generally positive order in $O_2(g)$, the observed increase in thin-film oxidation rate at very high oxygen pressure is as expected.

For oxygen exposures of 10^3-10^7 L, oxidation of thick Sn films proceeds as a single rapid process; for a 3.4 ML Sn overlayer this results in oxidation of ~45% of the initial Sn. Sn multilayers (>2 ML) form 3D crystallites with average island heights in excess of 10 ML.[22] Hence the faster, low-pressure oxidation kinetics observed over such crystallites may reflect a higher density of reactive defect sites compared with their smooth 2D counterparts formed at lower Sn coverages. Differences in the thermodynamic stabilities of low-dimensional versus extended tin oxide structures (resulting from the oxidation of submonolayer and multilayer Sn

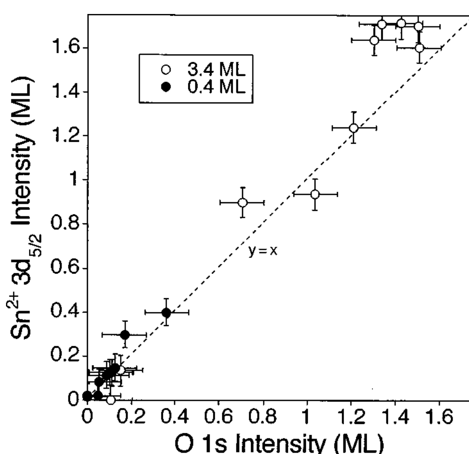

FIG. 7. Sn^{2+} $3d$ intensity vs O $1s$ intensity as a function of oxygen coverage for 0.4 and 3.4 ML Sn films.

films, respectively) due to differences in, e.g., Madelung potential, may also facilitate low-pressure oxidation of thicker Sn overlayers.

Deconvolution of the Sn XP spectra shows that a significant fraction of Sn in multilayer films remains in metallic form following 300 K oxidation. The lower intensity of the Sn^0 versus Sn^{2+} emission is consistent with diffusion-limited oxygen transport to Sn atoms at the Pd/Sn interface, suggesting that Sn oxidation is kinetically controlled at 300 K. Metallic Sn atoms are thus protected beneath a capping, passivating oxide layer. Paffet *et al.* report similar behavior upon low-pressure 300 K oxidation of a 5 ML Sn deposit on Pt(111).[33]

Although the greater thermodynamic stability of SnO_2 over SnO favors higher oxide formation over bulk Sn at high oxygen exposures,[34] where diffusion limitations may be lifted, recent high-pressure studies report the presence of SnO, in addition to SnO_2, even after exposures of 8×10^{11} L O_2.[19] Furthermore, EELS measurements indicate that oxidation of both polycrystalline Sn foil[7] and thin Sn overlayers (1–9 ML) on Au(111) (Ref. 27) results in subsurface SnO_2 residing beneath a capping SnO-rich layer. Our results (Fig. 7) show that the stoichiometry of the tin oxide formed from both submonolayer and multilayer films is independent of Sn film thickness. However, it must be remembered that the very thin films discussed in this work may exhibit markedly different behavior to that found during oxidation of bulk polycrystalline tin, where diffusion-limited oxygen transport may induce strong depth-dependent gradients in oxide stoichiometry.

By calibrating the fraction of tin present as oxide (Fig. 6) against the known as-deposited Sn coverage, and converting the corresponding O *KLL* AES signal into effective monolayers of surface oxygen (see Sec. II), we identify the surface oxide formed in the present study as SnO and not SnO_2. It must be noted that the use of low-energy ELS and valence-band spectra provide valuable alternative methods of fingerprinting the stoichiometry and quality character of tin oxides illustrated by the work of Hoflund[12,7,6] and Themlin,[31] respectively. In the present study, electron loss spectroscopy (ELS) measurements were unavailable, while XP valence-band spectroscopy proved unhelpful due to the intense substrate $4d$,$5sp$ bands at the Fermi edge, which obscure the Sn $5s$ and O $2p$ transitions.

Additional evidence that SnO is the oxidation product for all Sn films and oxidation treatments is provided by comparison of the Sn photoemission parameters with reference data (Table I). Upon oxidation of bulk Sn samples, Powell[11] found identical Sn *MNN* AES shifts of ~5.5 eV for SnO and SnO_2, while Sen *et al.*[16] observed a 4 eV shift. More recent work dealing with SnO films grown on a variety of substrates reports reproducible shifts ~2 eV less than observed for their SnO_2 counterparts.[27,35] The small (~2 eV) shifts found here [Fig. 8(a)] therefore point to formation of SnO rather than SnO_2, and are similar to those (2.7–3 eV) found during oxidation of *thin* ($\leqslant$8 ML) Sn films on Au(111).[27] Similarly, despite discrepancies in reported Sn $3d$ BE shifts between Sn metal and SnO versus SnO_2, which range from 1–1.8 and 1.8–2.5 eV, respectively,[19,28] our limiting shift of ~1 eV [Fig. 8(b)] is again consistent with lower oxide formation. (Recent studies suggest a shift of up to 0.7 eV between the Sn core levels in bulk SnO and SnO_2,[31,28] although consensus favors a smaller separation of 0.18–0.5 eV.[23,36] These disagreements illustrate the importance of using reliable methods to calibrate or fingerprint tin oxide stoichiometries.)

While the initial (unoxidized) Sn $3d$ BE in Fig. 8(b) is comparable to that reported in the literature (Refs. 28, 31, and 35), that of the 0.4 ML film is also enhanced by strong interfacial charge transfer to Pd, and the reduced final-state core-hole screening associated with the cluster→bulk transition observed for small supported metal clusters.

Another indicator of the Sn chemical state, the modified Sn Auger parameter ($\alpha' = \mathrm{BE\ Sn}\ 3d_{5/2} + \mathrm{KE\ Sn}MNN\mathrm{AES}$) was also evaluated [Fig. 8(c)]. Recent work shows that this quantity provides a reliable means of distinguishing SnO from SnO_2,[24,28,35] when a single chemical state is present. In the present case, although the Sn $3d$ XP core-level spectra are readily deconvoluted to reveal the positions of component states, such procedures cannot be easily applied to the corresponding Auger transitions. The values of α' shown in Fig. 8(c) are thus only truly valid for the extremes of as-deposited and fully oxidized films. The quantitative analysis presented in Fig. 6 reveals that only submonolayer films exhibit such complete oxidation. For a 0.4 ML oxidized Sn film the limiting Auger parameter shift of ~1.4 eV is significantly smaller than values determined from comparison of bulk polycrystalline Sn samples with either bulk SnO or SnO_2 standards, for which $\Delta\alpha'$ varies between ~2.3 and 3.7 eV.[28,37] Auger parameter shifts for SnO samples are typically 1 eV smaller than their SnO_2 counterparts.[28] The values measured in the present study are thus indicative of formation of lower oxide SnO_x ($x<2$), *although the low dimensionality of these surface oxides is expected to reduce* $\Delta\alpha'$ *below values predicted for formation of either bulk oxide (see below).* Unequivocal assignment of the limiting oxide stoichiometry based solely on the measured Auger parameters is thus not possible in this study. It is also important to note that the Sn $3d_{5/2}$ FWHM of 2.0 eV used to fit the oxide component is similar to that reported by Themlin *et al.* for a pure SnO surface,[31] but significantly greater than that of single-crystal SnO_2 (1.4 eV).[31] This supports our assignment of a SnO surface oxide in this study. The limiting oxygen

TABLE I. Comparison of Sn XP binding energies, Auger kinetic energies, and Auger parameters for bulk and supported thin-film tin oxides.

Phase	E_b $3d_{5/2}$	ΔE_b E_b (Sn)	E_k $M_5N_{45}N_{45}$	ΔE_k	α'	Ref.
Sn^0 (>10 ML)	483.8		430		915.4	This work
Sn	483.8					31
Sn	484.9		430		914.9	28
Sn	484.65					12
Sn			429			45
0.4 ML SnO_x/Pd(111)	485.3	0.8	428	2	913.8	This work
3.4 ML SnO_x/Pd(111)	485	0.9	427.7	2.3	914	This work
2 ML SnO_x/Au(111) (+6×10^{+6} L O_2)			428	3.8		27
9 ML SnO_x/Au(111) (+6×10^{+6} L O_2)			429	2.7		27
5 ML SnO_x/Pt(111) (+500 L O_2)	485.8	1				33
SnO	485.6	1.8				31
SnO	486.4	1.5	426.2	3.8	912.6	28
SnO	486.9					37
SnO_x ($x=1-2$)	485.7	1.05		5	910.7	12
SnO_2	486.3	2.5				31
SnO_2	487.1	2.2	424.2	5.8	911.2	28
SnO_2	486.4	1.75		5	909.7	12
SnO_2	486.6		424.6		919.2	37

Auger parameter derived from the O 1s and O *KLL* transitions of ~1041 eV is also in accord with SnO reference data.[28,35]

The Sn Auger and XP core-level shifts that we attribute to formation of stoichiometric SnO are smaller than those reported between bulk Sn metal and bulk SnO.[19,28,31] These differences may reflect two factors. First, the electronic properties of the as-deposited Sn overlayers on Pd(111) are perturbed relative to their bulk values by (i) reduced final-state screening within small Sn islands and (ii) initial-state charge transfer from Sn→Pd.[22] Both contributions increase the Sn metal core-level binding energies, thus reducing the observed shift upon oxidation. Analysis of the Sn Auger parameter shift, $\Delta\alpha'$, confirms there is little change in the Sn local electronic environment as a result of oxidation. With the usual approximation that $\Delta\alpha'=2\Delta\mathrm{RE}$ (where ΔRE is the difference in extra-atomic final-state core-hole relaxation energy between environments), the initial-state charge redistribution ($\Delta\varepsilon$) due to oxidation is given by

$$\Delta\mathrm{BE}=\Delta\varepsilon-\Delta\mathrm{RE}.$$

Taking the limiting value of $\Delta\alpha'$ as -1.4 eV for both submonolayer and multilayer Sn films, and corresponding ΔBE of +0.7–0.9 eV, we calculate $\Delta\mathrm{RE}=-0.7$ eV and $\Delta\varepsilon=0.2$ eV. Hence oxide formation is accompanied by a large decrease in the efficiency of core-hole screening, in line with expectation, but relatively little change in the initial-state charge density of Sn atoms in the thin film. The changes in substrate photoemission features suggest that *oxidation of metallic Sn overlayers eliminates the strong electronic interaction between interfacial Pd and Sn atoms*. Hence the sub-

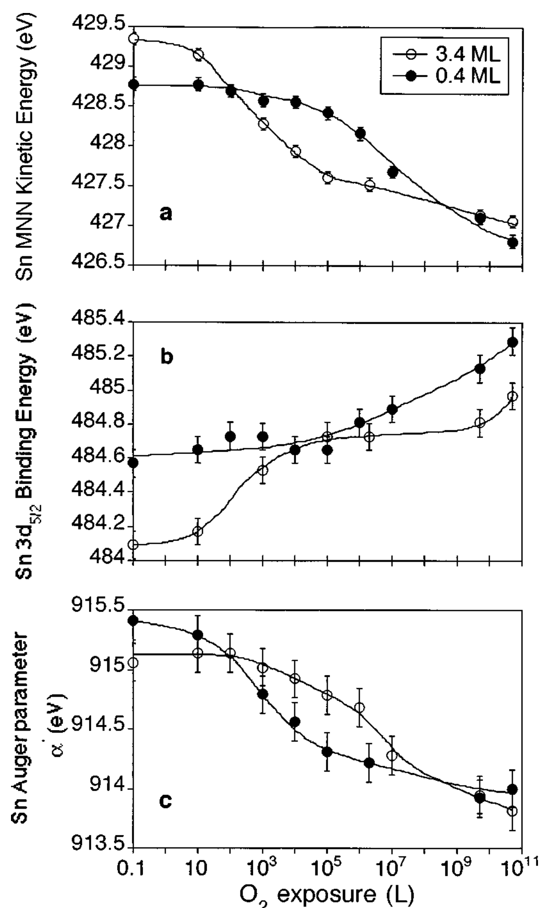

FIG. 8. Combined Sn. (a) *MNN* KE, (b) 3d BE, and (c) Auger parameter vs oxygen exposure for 0.4 and 3.4 ML Sn films.

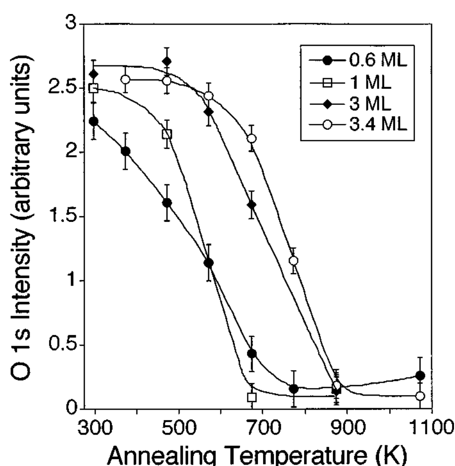

FIG. 9. O 1s XP intensities vs annealing temperature as a function of tin oxide film thickness (300 K oxidation, 5×10^{10} L O_2).

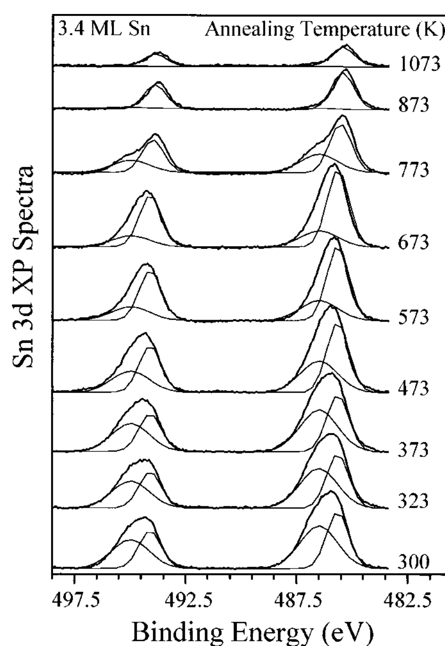

FIG. 10. Sn 3d XP spectra as a function of annealing temperature for a 3.4 ML oxidized Sn film (300 K oxidation, 5×10^{10} L O_2). Fitted metal and oxide Gaussian components are also shown.

strate does not appear to influence the electronic properties of surface tin oxide. A second factor acting to reduce the oxidation-induced BE shift of Sn thin films relative to their bulk counterparts could be differences in the respective Madelung potential contribution. That is, *the influence of oxygen anion neighbors on Sn sites may be greater for low dimensional, oxygen-terminated films than for extended 3D oxide structures*.

Oxidation may also induce morphological transformations in metal overlayers, e.g., cracking of thin films to expose substrate patches,[38] or conversely the spreading of metal crystallites into a continuous oxide film. The increased attenuation of substrate emission that we observe upon oxidation of submonolayer and multilayer Sn films eliminates the former possibility. The predicted attenuation of Pd emission due to oxidation of a 3.4 ML Sn film may be modeled for the case of a continuous capping SnO overlayer and equivalent underlying Sn metal phase according to De Padova *et al.*[19] Taking the monolayer thickness of Sn and SnO as ~2.33 and 2 Å, respectively, and the combined Sn/SnO overlayer as ~7.5 Å, the attenuation of the Pd 3d signal (relative to the clean surface) is predicted as ~55%. This value is significantly higher than the measured attenuation of ~35%, suggesting that oxidation induces incomplete spreading of the metallic Sn islands, i.e., the process stops short of coalescence into a continuous oxide film.

IV. THERMAL STABILITY OF OXIDIZED OVERLAYERS

In vacuo annealing of oxidized Sn overlayers was performed between 300 and 1100 K to investigate their decomposition and the possibility of alloy formation. Heating was carried out for 1 min intervals at the specified temperatures, after subjecting the sample to 5×10^{10} L O_2, subsequent spectroscopic measurements were performed at 300 K.

Multilayer films remain unperturbed for annealing temperatures <473 K, whereas submonolayer films evolved even at 373 K. In every case, annealing induced a decrease in the O XAES and XP intensities (Fig. 9) such that the onset temperature and that at which the oxygen signal attained its limiting value increased with SnO_x overlayer thickness. Thus for Sn deposits with initial loading varying from 0.6 to 3.4 ML, the onset temperature for oxygen loss and that corresponding to limiting oxygen loss varied between ~373–673 K and 673–1100 K, respectively. This decrease in surface oxygen is accompanied by evolution of gaseous oxygen (as detected by quadrupole mass spectrometer), and a concomitant rise in Pd photoemission signals, which recover their clean surface intensities above 1000 K. It is apparent from Fig. 9 that oxide stability increases with film thickness, although for annealed tin oxide multilayers we cannot discount possible migration of some oxide into the selvedge region at temperatures below which oxygen is evolved. Such reversible thermally induced migration of oxide overlayers has been observed for thick titania overlayers on polycrystalline Pt.[39]

The Sn Auger and XP peak intensities are also invariant at temperatures <473 K, decreasing smoothly between 500 and 900 K to a common nonzero limiting value. This process is illustrated for a 3.4 ML oxidized film in Fig. 10. Loss of surface Sn is accompanied by a respective increase and decrease in the Sn MVV kinetic energy and Sn 3d binding energy, Figs. 11(a) and 11(b). These shifts are more pronounced for submonolayer SnO_x films (~0.8 eV) than for their multilayer counterparts (~0.3 eV). The Sn Auger parameter dependence on annealing temperature and overlayer thickness is also shown in Fig. 11(c). For thin films α' rises rapidly, reaching ~915.2 eV by 873 K. Conversely, α' for thick overlayers remains constant <673 K, before rising to the same limiting value by 1073 K.

These observations demonstrate that heating of Pd supported SnO_x films induces a progressive reversal of the trends observed during oxidation of all overlayers. Vacuum annealing thus provides an efficient means of reducing Pd-supported tin oxide films, analogous to the behavior reported on Pt surfaces.[32] The coverage dependence of both substrate and overlayer photoemission features shows that the thermal stability of supported tin oxide films increases with film

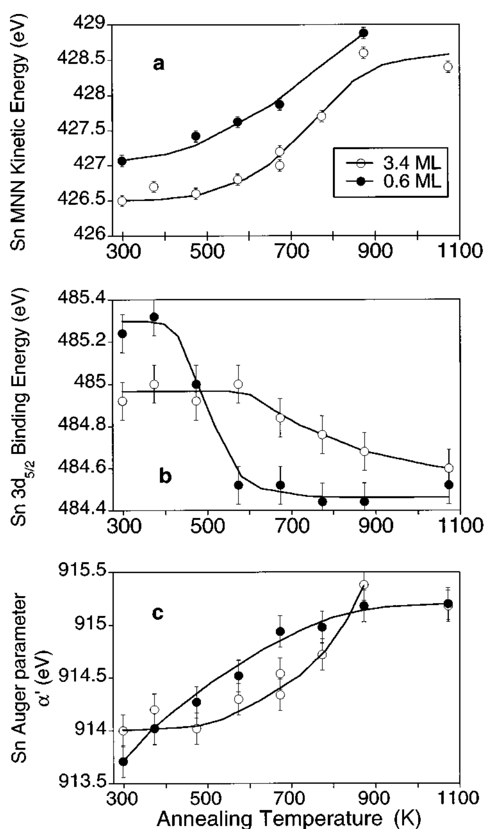

FIG. 11. Combined Sn. (a) *MNN* KE, (b) $3d$ BE, and (c) Auger parameter vs oxygen exposure for 0.6 and 3.4 ML oxidized Sn films (300 K oxidation, 5×10^{10} L O_2).

thickness. Thus submonolayer stoichiometric SnO films decompose at temperatures as low as 473 K, being fully reduced by ~673 K. In contrast, multilayer oxide films remain stable to ~573 K, and are fully decomposed only above 873 K; note that bulk SnO is stable to ⩾1000 K.

While annealing is clearly accompanied by the reduction of tin oxide to the metal, *the concurrent loss of surface Sn indicates diffusion and Sn/Pd intermixing*. This is in accord with recent work,[22] which shows that on heating, Sn overlayers do not desorb from Pd(111); instead, intermixing and crystalline surface alloy formation occurs. Alloying reduces Pd-Pd orbital overlap and also leads to significant initial-state charge transfer from Sn→Pd (Ref. 22) and accompanying Pd $4d\rightarrow5s,5p$ charge redistribution, as observed in related systems.[40] Both effects act to reduce the efficiency of Pd $3d$ core-hole screening, and thus FWHM, with respect to the clean surface. Since thin metallic Sn overlayers induce Pd core-level *broadening* by enhancing the Pd surface core-level shift (SCLS) from ~0.25 (Ref. 29) to 0.5 eV,[22] the Pd $3d$ FWHM provides a sensitive indicator of Pd/Sn alloying. Figure 12 shows that the Pd FWHM's exhibit a strong dependence on annealing temperature, decreasing from the clean surface value (~1.44 eV) to minima between 673 and 773 K. The depth and corresponding temperature of these minima increase with oxide thickness; the same trends are observed during heating of metallic Sn overlayers on Pd(111), leading to formation of monolayer Pd_2Sn or multilayer Pd_3Sn surface alloys.[22] It is interesting to note that vacuum annealed Pd-doped SnO_2 surfaces also produce interfacial Pd-Sn alloys.[41] *It therefore seems likely that exothermic alloy formation plays a role in determining the thermal stability of tin oxide overlayers on Pd.* In addition, submonolayer oxide films are strongly destabilized with respect to both multilayer and bulk oxides. This may reflect the lower lattice energy of their low dimensional structure compared to thicker or bulk material.

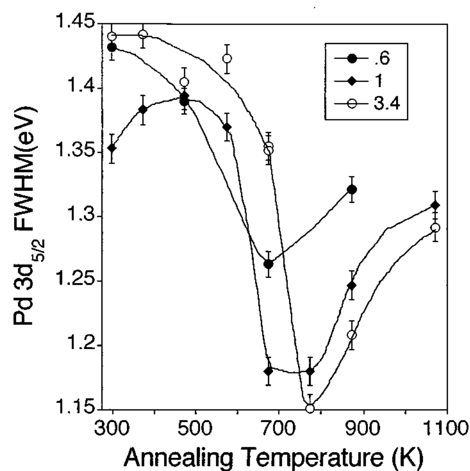

FIG. 12. Pd $3d$ FWHM vs annealing temperature as a function of tin oxide film thickness (300 K oxidation, 5×10^{10} L O_2).

Factor analysis of the Sn $3d$ spectra again indicates that for all oxide films only two tin species are present during the annealing process. Indeed, good quality fits were obtained using only one or two doublet Gaussian functions for all spectra, again fixing the peak energies for all but the highest temperature anneals. The onset of Pd/Sn alloying increases metallic Sn binding energies at these temperature as documented.[22] Spectral deconvolution using multiple oxide components to simulate the coexistence of, e.g., Sn^{2+} and Sn^{4+} phases did not improve the peak fits. We thus again associate the two Sn species with metallic Sn^0 (FWHM=1.1 eV) and oxidic Sn^{x+} (FWHM=1.9 eV), and the variations in their relative intensities with temperature and film thickness are shown in Fig. 13. Evidence that the starting SnO stoichiometry is maintained during the decomposition process is apparent from a plot of the Sn^{x+} signal

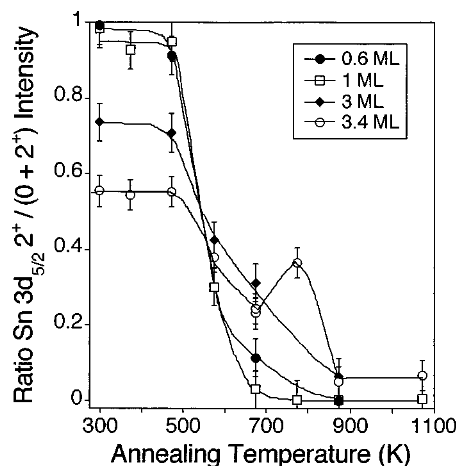

FIG. 13. Ratio of Sn^{2+}:Sn^0 $3d$ XP intensities vs annealing temperature for 0.4 and 3.4 ML oxidized Sn films (300 K oxidation, 5×10^{10} L O_2).

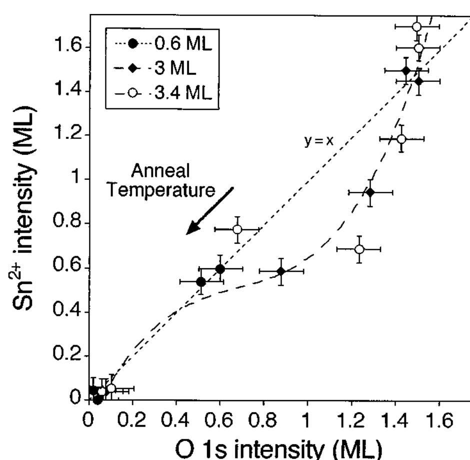

FIG. 14. Sn^{2+} $3d$ intensity vs O $1s$ intensity as a function of annealing temperature for 0.4 and 3.4 ML oxidized Sn films (300 K oxidation, 5×10^{10} L O_2).

against the corresponding O $1s$ signal (Fig. 14), after calibration against appropriate tin and oxygen standards (see Sec. II). With the exception of multilayer films annealed to 773 K, these plots are consistent with direct reduction of SnO→Sn. This contrasts with the reduction of bulk SnO samples, wherein disproportionation occurs to form SnO_2 above 573 K [via an Sn_2O_3 (Ref. 42) or Sn_3O_4 (Ref. 43) intermediate], followed by eventual metallic Sn formation at >873 K. However this bulklike behavior *is* recovered for multilayer films, for which the temperature-dependent Sn^{x+}:O stoichiometry indicates intermediate oxide formation ($SnO_{x=1-2}$) at ~800 K.

A notable feature during annealing of multilayer (>3 ML) tin oxide films is the surprising reemergence of oxidic features at temperatures ~800 K (Fig. 10), following a regime during which the surface oxide concentration is halved (Fig. 9). The increased oxide intensity and Sn $3d$ core-level shift are accompanied by the aforementioned decrease in Sn^{x+}:O $1s$ ratio, and result in a highly asymmetric peak envelope (Fig. 10), though both oxide and metal components themselves retain symmetric Gaussian line shapes. Together these changes may reflect increased oxygen mobility, resulting in stabilization of some Sn within a (thermodynamically) more stable higher oxide structure.[42] Still higher temperatures continuously raise the interdiffusion rates of the surface metallic Sn phase, facilitating the sharp rise in the observed relative intensities of oxidic versus metallic features. Similar Sn interdiffusion and the concomitant SnO_2 formation is reported following *in vacuo* annealing of 300 K oxidized Sn deposits on Au(111).[44] Here, since the BE shifts and associated Auger parameter of the higher oxide are less than expected for bulk SnO_2,[28,37] it is possible that the observed changes reflect the formation of a metastable intermediate (e.g., Sn_3O_4).

V. CONCLUSIONS

(i) Submonolayer Sn films readily undergo complete oxidation at 300 K following oxygen exposure ($\sim10^{11}$ L), while oxidation of thicker films appears limited by oxygen diffusion. Relative rates of oxygen uptake increase with Sn film thickness, though the degree of oxidation decreases. However, the composition of capping layer tin oxide is independent of the initial Sn loading.

(ii) XPS analysis indicates that 300 K oxidation always generates SnO rather than SnO_2. However, thermal decomposition of these SnO films involves disproportionation via a higher oxide, possibly Sn_3O_4.

(iii) Oxidation leads to relatively little change in initial state valence charge density on Sn, an effect that may in part be due to the low dimensionality of the oxide film.

(iv) The oxide films decompose with evolution of gaseous oxygen to form well-ordered Pd/Sn surface alloys. Their thermal stability is markedly less than that of the bulk material but increases substantially with increasing film thickness, the decomposition temperature rising with thickness from ~600 K (submonolayer) to ~800 K (multilayers). Exothermic Pd/Sn alloying may thus promote the redox chemistry of tin oxide films.

ACKNOWLEDGMENTS

The authors are grateful to Juan Pedro Holgado for assistance with the factor analysis. This work was supported under Grant No. GR/K 45562 awarded by the UK EPSRC. We thank Johnson Matthey plc for a loan of precious metals.

*Present address: School of Chemistry, University of Hull, Hull HU 6 7RX, England.
†Author to whom correspondence should be addressed.

[1] J. Vetrone, Y. W. Chung, R. E. Cavicchi, and S. Semancik, J. Appl. Phys. **73**, 8371 (1993).
[2] W. P. Kang and C. K. Kim, J. Appl. Phys. **75**, 4237 (1994).
[3] V. A. Gercher, D. F. Cox, and J. M. Themlin, Surf. Sci. **306**, 279 (1994).
[4] M. J. Fuller and M. E. Warwick, J. Catal. **29**, 441 (1973).
[5] A. F. Lee, C. J. Baddeley, G. D. Moggridge, R. M. Ormerod, R. M. Lambert, J.-P. Candy, and J.-M. Basset, J. Phys. Chem. **102**, 2797 (1997).
[6] D. F. Cox and G. Hoflund, Surf. Sci. **151**, 202 (1985).
[7] G. B. Hoflund and G. R. Corallo, Phys. Rev. B **46**, 7110 (1992).
[8] W. E. Boggs, R. H. Kachik, and G. E. Pellissier, J. Electrochem. Soc. **108**, 1 (1961).
[9] R. A. Powell and W. E. Spicer, Surf. Sci. **55**, 681 (1976).
[10] C. M. Stander, Appl. Surf. Sci. **16**, 463 (1983).
[11] R. A. Powell, Appl. Surf. Sci. **3**, 397 (1979).
[12] D. A. Asbury and G. B. Hoflund, J. Vac. Sci. Technol. A **5**, 1132 (1987).
[13] C. L. Lau and G. K. Wertheim, J. Vac. Sci. Technol. **15**, 622 (1978).
[14] A. W. C. Lin, N. R. Armstrong, and T. Kuwana, Anal. Chem. **49**, 1228 (1977).
[15] C. D. Wagner and P. Biloen, Surf. Sci. **35**, 82 (1973).
[16] S. K. Sen, S. Sen, and L. Bauer, Thin Solid Films **82**, 157 (1981).
[17] A. J. Bevelo, J. D. Verhoeven, and M. Noack, Surf. Sci. **134**, 499 (1983).
[18] M. E. Woods and B. J. Hopkins, J. Phys. C **18**, 3255 (1985).
[19] P. De Padova, M. Fanfoni, R. Larciprete, M. Mangiantini, S. Priori, and P. Perfetti, Surf. Sci. **313**, 379 (1994).
[20] B. E. Handy, J. A. Dumesic, R. D. Sherwood, and R. T. K. Baker, J. Catal. **124**, 160 (1990).

[21] J. H. Horton, G. D. Moggridge, R. M. Ormerod, A. V. Kolobov, and R. M. Lambert, Thin Solid Films **237**, 134 (1994).
[22] A. F. Lee, C. J. Baddeley, M. S. Tikhov, and R. M. Lambert, Surf. Sci. **373**, 195 (1997).
[23] M. A. Stranick and A. Moskwa, Surf. Sci. Spectra **2**, 50 (1993).
[24] V. M. Jimenez, J. A. Mejias, J. P. Espinos, and A. R. Gonzalez-Elipe, Surf. Sci. **366**, 545 (1996).
[25] H. Conrad, G. Ertl, J. Kuppers, and E. E. Latta, Surf. Sci. **65**, 245 (1977).
[26] S. C. Barlow, P. Bayat-Mokhtari, and T. E. Gallon, J. Phys. C **12**, 5577 (1979).
[27] Y. Zhang and A. J. Slavin, J. Vac. Sci. Technol. A **10**, 2371 (1992).
[28] L. Kovar, Zs. Kovacs, R. Sanjines, G. Moretti, G. Margaritondo, J. Palinkas, and H. Adachi, Surf. Interface Anal. **23**, 467 (1995).
[29] J. N. Andersen, D. Hennig, E. Lundgren, M. Methfessel, R. Nyholm, and M. Scheffler, Phys. Rev. B **50**, 17 525 (1994).
[30] C. T. Campbell, D. C. Foyt, and J. M. White, J. Phys. Chem. **81**, 491 (1977).
[31] J.-M. Themlin, M. Chtaib, L. Henrard, P. Lambin, J. Darville, and J.-M. Gilles, Phys. Rev. B **46**, 2460 (1992).
[32] S. D. Gardener, G. B. Hoflund, M. R. Davidson, and D. R. Schryer, J. Catal. **115**, 132 (1989).
[33] M. T. Paffett, S. C. Gebhard, R. G. Windham, and B. E. Koel, J. Phys. Chem. **94**, 6837 (1990).
[34] *CRC Handbook of Chemistry and Physics*, 69th ed., edited by R. C. Weast (The Chemical Rubber Company, Cleveland, 1988), p. D-90; P. W. Atkins, in *Physical Chemistry*, 3rd ed. (Oxford University Press, Oxford, 1989), p. 819.
[35] V. M. Jimenez, J. P. Espinos, and A. R. Gonzalez-Elipe, Surf. Sci. **366**, 556 (1996).
[36] E. Paparazzo, G. Fierro, G. M. Ingo, and N. Zacchetti, Surf. Interface Anal. **12**, 438 (1988).
[37] D. Briggs and M. P. Seah, in *Practical Surface Analysis* (Wiley, New York, 1990), Vol. 1, Appendix 5.
[38] P. Legare, F. Finck, R. Roche, and G. Maire, Surf. Sci. **217**, 167 (1989).
[39] R. J. Gorte, E. Altman, G. R. Corallo, M. R. Davidson, D. A. Asbury, and G. B. Hoflund, Surf. Sci. **188**, 327 (1987).
[40] J. A. Rodriguez and M. Kuhn, Chem. Phys. Lett. **240**, 435 (1995).
[41] G. E. Poirier, R. E. Cavicchi, and S. Semancik, J. Vac. Sci. Technol. A **12**, 2149 (1994).
[42] M. S. Moreno, R. C. Mercader, and A. G. Bibiloni, J. Phys.: Condens. Matter **4**, 351 (1992).
[43] F. Gauzzi, B. Verdini, A. Maddalena, and G. Principi, Inorg. Chim. Acta **104**, 1 (1985).
[44] Y. Zhang and A. J. Slavin, Phys. Rev. B **49**, 2005 (1994).
[45] C. D. Wagner, in *Practical Surface Analysis*, edited by D. Briggs and M. P. Seah (Wiley, New York, 1990), Vol. 1, p. 648.